*American Mineralogist, Volume 84, pages 1384–1391, 1999*

# Structures of $FeTiO_3$ (0001) surfaces observed by scanning tunneling microscopy

**ROBERT A. FELLOWS,[1,*] ALISTAIR R. LENNIE,[1] ANDREAS W. MUNZ,[2] DAVID J. VAUGHAN,[1] AND GEOFF THORNTON[3]**

[1]Department of Earth Sciences, University of Manchester, Oxford Road, Manchester M13 9PL, U.K.
[2]Department of Inorganic Chemistry, Fritz-Haber Institut der Max-Planck Gesellschaft, Faradayweg 4-6, D-14195, Berlin, Germany
[3]Interdisciplinary Research Centre in Surface Science and Department of Chemistry, University of Manchester, Oxford Road, Manchester M13 9PL, U.K.

## ABSTRACT

Scanning tunneling microscopy (STM) was used to investigate the (0001) surface structure of a natural single crystal of $FeTiO_3$, following argon-ion sputtering and annealing in $O_2$. Low energy electron diffraction (LEED) of the $FeTiO_3$ (0001) surface shows two different diffraction patterns that depend on preparation. We examined surfaces with a hexagonal pattern that was interpreted as a $(1 \times 1)$ bulk termination. Wide-scale STM images of the $(1 \times 1)$ bulk termination show two distinct co-existing areas: large atomically rough terraces and small, smoother, atomically resolved areas within. The observed single step height of $2.2 \pm 0.3$ Å (doubled values are also found) plus data from the surface orientation implies that two termination types are seen on the (0001) surface after initial stages of preparation, and that these are either cation-terminated surface planes ($Fe^{2+}$ or $Ti^{4+}$) or close-packed oxygen terminations. Atomic-resolution STM images of smooth terrace areas show features arranged in a hexagonal array, with a separation of $4.8 \pm 0.2$ Å. A model is proposed that identifies this termination as an unreconstructed (0001) termination of $FeTiO_3$ that exposes half a layer of either $Fe^{2+}$ or $Ti^{4+}$ cations over a close-packed O layer, with each feature arising from a trimer of O atoms capped by a single cation ($Fe^{2+}$ or $Ti^{4+}$).

## INTRODUCTION

Iron-titanium oxide minerals are of importance in many geological environments and are stable over a wide range of temperatures and redox conditions (Waite 1990). Phases in the ilmenite ($FeTiO_3$)-hematite ($\alpha$-$Fe_2O_3$) solid solution series, which are stable under moderately reducing conditions, show interesting magnetic properties and, with the exception of magnetite ($Fe_3O_4$), are the most important carriers of remanent magnetization in natural materials (Brown and Navrotsky 1993). Ilmenite ($FeTiO_3$) is also economically important as the major source of Ti for the commercial production of $TiO_2$.

Although numerous studies of the Fe-Ti-O system have addressed questions concerning crystal structure and phase transformations (Lindsley 1976a, 1976b), electrical properties (Andreozzi et al. 1996), and magnetic properties (Shirane et al. 1959), few studies have been undertaken on the surface structure and chemistry of the Fe-Ti oxides. Complex and intriguing surface properties are found in both Ti-O and Fe-O systems. For example, in the Ti-O system, rutile ($TiO_2$) (110) and (100) surfaces prepared by $Ar^+$ sputtering and annealing in ultra high vacuum ($\leq 1 \times 10^{-10}$ mbar) at temperatures in the range 870 K to 1200 K produce a variety of surface reconstructions (e.g., Murray et al. 1994; Berkó et al. 1996; Leibsle et al. 1997). In the Fe-O system, hematite ($\alpha$-$Fe_2O_3$) (0001) surfaces prepared by $Ar^+$ sputtering and annealing in $1 \times 10^{-6}$ mbar $O_2$ at 1000 K form a magnetite ($Fe_3O_4$) (111) termination (Condon et al. 1994). $Fe_3O_4$ (111) surfaces following $Ar^+$ sputtering and annealing in ultra high vacuum at 1100 K form biphase ordering of $Fe_3O_4$ (111) and $Fe_{1-x}O$ (111) islands (Condon et al. 1997). Research on Fe-O thin films deposited on (111) and (100) surfaces of Pt single crystals also shows structural variations dependent on oxygen partial pressure and thin-film thickness (Weiss et al. 1993; Galloway et al. 1996; Weiss 1997; Kim et al. 1997; Ritter et al. 1997, 1998). This variety of surfaces suggests that the exploration of surface structures and properties of Fe-Ti-O phases offers the potential for discovering new types of surface behavior.

This study presents scanning tunneling microscopy (STM) images of the $FeTiO_3$ and builds on an earlier low energy electron diffraction (LEED) study of this surface (Fellows et al. 1997). The STM images reported here are the first STM images of the $FeTiO_3$ (0001) surface.

The $FeTiO_3$ structure (space group $R\bar{3}$) is derived from $\alpha$-$Fe_2O_3$ by replacing every other layer of Fe atoms in the (0001) planes by a layer of Ti atoms, thus producing alternating layers of Fe and Ti atoms between (slightly distorted) hexagonally close-packed O layers (see e.g., Klein and Hurlbut 1993). The hexagonal unit cell has dimensions $a = 5.089$ Å, $c = 14.163$ Å. The formal valence of metal ions in this structure is given by the formula $Fe^{2+}Ti^{4+}O_3$. A view normal to [0001] in the bulk $FeTiO_3$ structure (Fig. 1) shows within each bulk cation layer two cation positions, either high or low in the [0001] direction. High-positioned cations are labeled A and low positioned cations are labeled B in this figure.

*E-mail: rafellows@hotmail.com

0003-004X/99/0009–1384$05.00

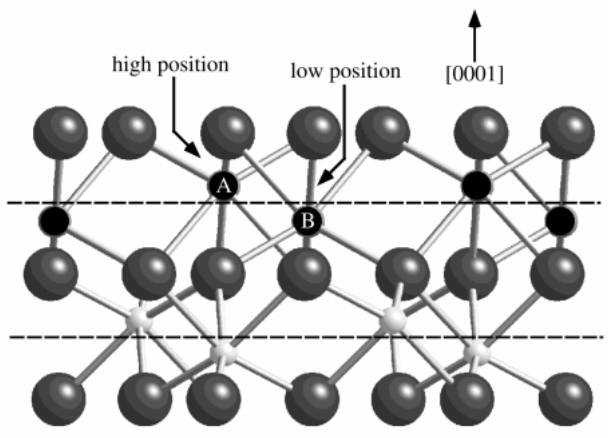


**FIGURE 1.** Schematic illustration showing the bulk $FeTiO_3$ structure projected along [11$\bar{2}$0]. Layers of O atoms represented by large gray spheres, Ti atoms by small gray spheres, and Fe atoms by small black spheres. In this projection the metal atoms are aligned normal to the plane shown. Within the cation layers, two locations for the cations are observed, high position (labeled A) and low position (labeled B). The stable termination planes of the (0001) bulk surface, which divide the cation layers in two, are shown as dashed lines. The [0001] direction of the bulk structure is shown.

A LEED study of the $FeTiO_3$ (0001) surface shows that this surface can produce two different diffraction patterns depending on preparation (Fellows et al. 1997). The first (hexagonal) pattern is interpreted as a $(1 \times 1)$ bulk termination. The second pattern, containing additional spots with their first zone vectors rotated 30° from the directions of the substrate, is consistent with either a $(2/\sqrt{3} \times 2/\sqrt{3})$ R 30° surface reconstruction, or a spinel-type (111) surface termination.

## EXPERIMENTAL PROCEDURE

Measurements were carried out under UHV conditions in a chamber equipped with LEED, Auger electron spectroscopy and STM (Omicron, GmbH, Germany) facilities, and operating with a base pressure of $1 \times 10^{-10}$ mbar. The $FeTiO_3$ crystal, a natural sample from Ilmen, Russia, which exhibited well-developed faces, was cut and polished (1 μm) to within 0.5° of the (0001) plane, as determined by Laue diffraction. The 1.5 mm thick wafer was mounted on a Ta backplate using Ta clips, admitted to the vacuum chamber and degassed for 1 hour at 1073 K.

The $FeTiO_3$ (0001) surface was cleaned in situ by cycles of 500 eV $Ar^+$ bombardment at room temperature for 15 minutes, followed by annealing at 1073 K for 20 minutes in vacuum using electron-beam heating. This was then followed by two long anneals of 4 hours at 1073 K in $1 \times 10^{-7}$ mbar $O_2$. Auger electron spectroscopy indicated the presence of Fe, Ti, and O, with surface contamination below the level of detection.

A hexagonal $(1 \times 1)$ LEED pattern obtained following the sample preparation described above is shown in Figure 2. The first zone vectors of the electron diffraction spots are aligned with the $FeTiO_3$ substrate <10$\bar{1}$0> directions determined by Laue diffraction, as expected for a $(1 \times 1)$ termination of the (0001)

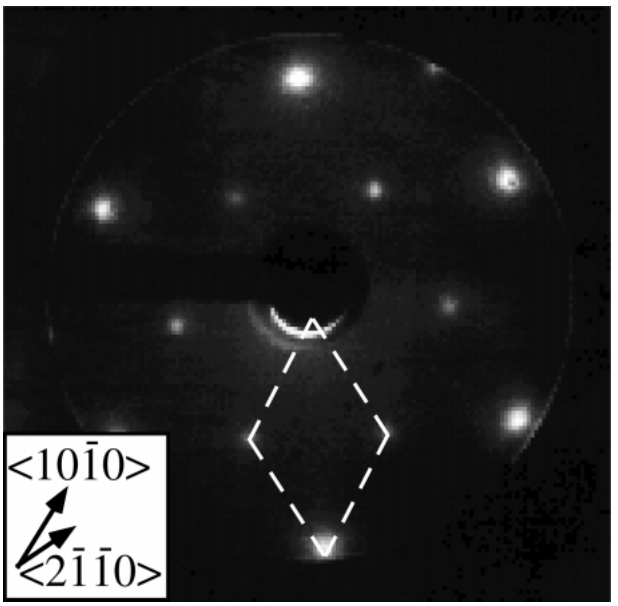


**FIGURE 2.** Low energy electron diffraction (LEED) pattern obtained from the $FeTiO_3$ (0001) crystal surface at 28 eV, after preparation by $Ar^+$ bombardment and annealing at 1073 K for 20 minutes in vacuum, followed by two long anneals of 4 hours at 1073 K in $1 \times 10^{-7}$ mbar $O_2$. The reciprocal surface unit cell is outlined. The crystallographic directions of the $FeTiO_3$ substrate from Laue diffraction are also shown.

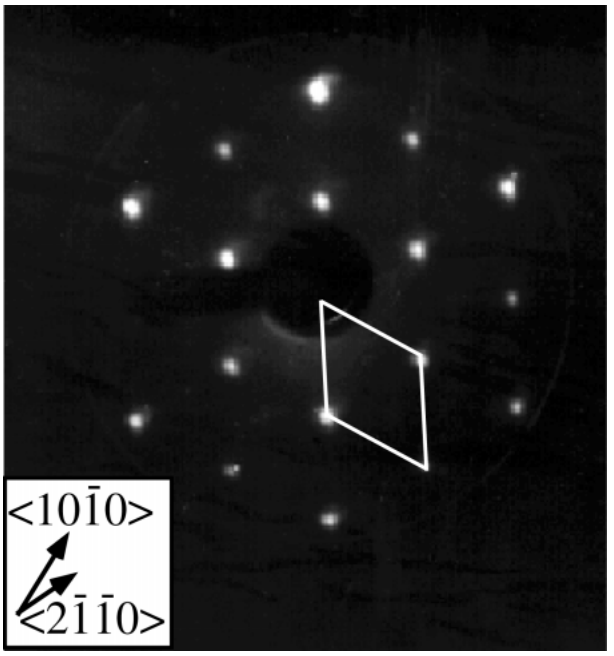


**FIGURE 3.** LEED pattern obtained from the $FeTiO_3$ (0001) crystal surface at 48 eV after preparation by $Ar^+$ bombardment followed by three 5 minute cycles of annealing at 1373 K in vacuum, with a fourth 5 minute annealing cycle at 1373 K in $1 \times 10^{-6}$ mbar $O_2$. This pattern, with first zone vectors rotated 30° from the <10$\bar{1}$0> directions, is consistent with either a $(2/\sqrt{3} \times 2/\sqrt{3})$ R 30° surface reconstruction or a spinel-type (111) surface termination. The reciprocal surface unit cell is outlined. The crystallographic directions of the $FeTiO_3$ substrate from Laue diffraction are also shown.

surface. This direction contains the closed spacing of O atoms. A second LEED pattern (Fig. 3), with first zone vectors rotated 30° from the <10$\bar{1}$0> directions, was observed following 500 eV $Ar^+$ bombardment at room temperature for 15 minutes, three 5 minute cycles of annealing at 1373 K in vacuum, and a fourth 5 minute annealing cycle at 1373 K in $1 \times 10^{-6}$ mbar $O_2$.

STM imaging used a tungsten tip ($Ar^+$ sputtered prior to use) and held at ground potential while the sample was biased. The images were recorded with the microscope operated in the constant current mode. Calibration of horizontal and vertical distances was achieved using STM images of Cu (110) ($2 \times 1$) O unit cells and monatomic steps (Coulman et al. 1990). Details of sample preparation prior to STM imaging are given for each of the images presented.

## Results and discussion

### Wide scale images

A typical STM image of the $FeTiO_3$ (0001) surface, which displays the ($1 \times 1$) type LEED pattern, is shown in Figure 4a. This image was obtained after $Ar^+$ sputtering for 15 minutes and annealing in $5 \times 10^{-7}$ mbar of $O_2$ for 5 minutes at 1373 K, followed by further annealing in vacuum at 1373 K for 3 minutes. Most of the image area shows large atomically rough terraces (labeled X) with small, smoother areas within them (labeled Y). The image also shows a high density of steps. Step heights between successive X terraces obtained from cross sections of the image (Fig. 4b) give values of $4.4 \pm 0.5$ Å. These values correspond to the separation between layers of the same atom type in the *c* direction of the bulk structure. The step from terrace X to terrace Y, or from Y to X, is $2.2 \pm 0.3$ Å, and corresponds to either the oxygen-oxygen or Fe-Ti separation in the *c* direction. These observed single step heights imply that two termination types are present on the (0001) surface following these initial stages of preparation.

Area type Y (Fig. 4a) only appears next to single step ($2.2 \pm 0.3$ Å) edges in these images. This suggests that these areas grow outward from step edges, across the rough terrace labeled X. Subsequent images (Fig. 5) show complete terraces of type Y with steps of $4.4 \pm 0.5$ Å to the next Y type terrace. This shows large terraces of both types and evidence of "domain-like" structures that are only found on the Y type terraces. These "domain-like" features have boundaries that are aligned along <2$\bar{1}\bar{1}$0>. These boundary features are at an elevation of $2.0 \pm 0.3$ Å above the surrounding surface.

Other areas imaged, which also display the ($1 \times 1$) type LEED pattern, show larger features. The image in Figure 6a has a surface unit cell with hexagonal symmetry and a periodicity of $29.2 \pm 2.5$ Å. The structure has a corrugation amplitude of about 0.5 Å, as shown by the profile. These structural features (Fig. 6) are similar to large-scale structures observed in STM images that have been interpreted as moiré patterns produced from higher order commensurability (Land et al. 1992) or lattice misfit (Wiederholt et al. 1995) between substrate and surface layers. The moiré superstructure theory has also been used to explain very similar images from FeO thin films grown on a Pt (111) substrate. Rotational mismatch between FeO bilayers and the underlying Pt (111) substrate cause large scale coincidence structures rotated relative to the ($1 \times 1$) unit cell of

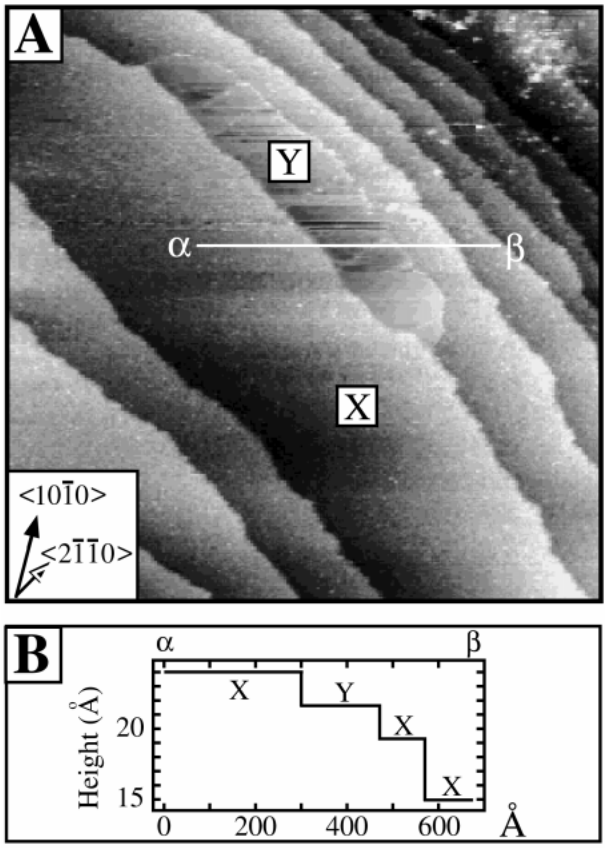


**Figure 4.** (**A**) A 1500 × 1500 Å constant current (sample bias 2.84 V, tunneling current 0.83 nA) STM image of an $FeTiO_3$ (0001) surface showing a high density of steps. Two types of surface area can be seen (labeled X and Y). This image was obtained following $Ar^+$ sputtering for 15 minutes and annealing in $5 \times 10^{-7}$ mbar of $O_2$ for 5 minutes at 1373 K, followed by further annealing at 1373 K in vacuum for 3 minutes. Most of the image is made up of rough terraces (labeled X), with smaller, smoother, areas (labeled Y). Crystallographic unit-cell directions of the substrate are indicated. (**B**) Schematic cross section of (**A**) along the line α-β showing step heights between terraces. The step height down from terrace X to Y, or Y to X is $2.2 \pm 0.3$ Å with the step down from terrace X to X being $4.4 \pm 0.5$ Å.

the Pt (111) substrate. These superstructures exhibit periodicities of between 22 and 38 Å, depending on the thickness of the FeO films (Ritter et al. 1998). STM images showing these types of superstructures, or related moiré fringes, have been interpreted as providing information about subsurface structure of the sample under investigation (Chevrier et al. 1996; Gai et al. 1996; Kobayashi 1996). The moiré superstructure patterns observed in images of the $FeTiO_3$ (0001) surface could be due either to a lattice mismatch between two layers rotated with respect to one another, or to a simple surface "superstucture" produced on the surface following annealing the sample in excess oxygen. In our experiment, the substrate is originally the same as the overlayer, and hence the formation of a moiré pattern suggests changes in oxygen stoichiometry either in the surface layer or in the substrate directly underneath. This indicates a process similar to

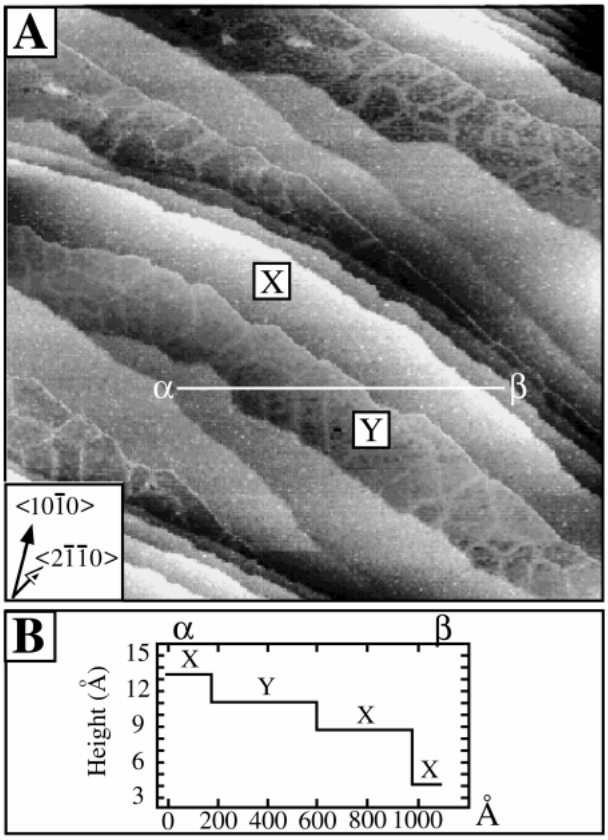


**FIGURE 5.** (**A**) A 2000 × 2000 Å constant current (sample bias 2.06 V, tunneling current 0.33 nA) STM image of an $FeTiO_3$ (0001) surface exhibiting surface types X and Y shown in Figure 5A. This image was obtained following the same preparation procedures as the sample used for image in Figure 5. There is evidence of "domain-like" surface structures within the areas labeled Y. These "domain-like" features have boundaries that are aligned along <2$\bar{1}\bar{1}$0>. These boundaries exhibit an elevation of 2.0 ± 0.3 Å above the surrounding terrace. (**B**) Schematic cross section of (**A**) along the line α-β showing steps between terraces. The step height down from terrace X to Y or Y to X, is 2.2 ± 0.3 Å with the step height between X terraces being 4.4 ± 0.5 Å.

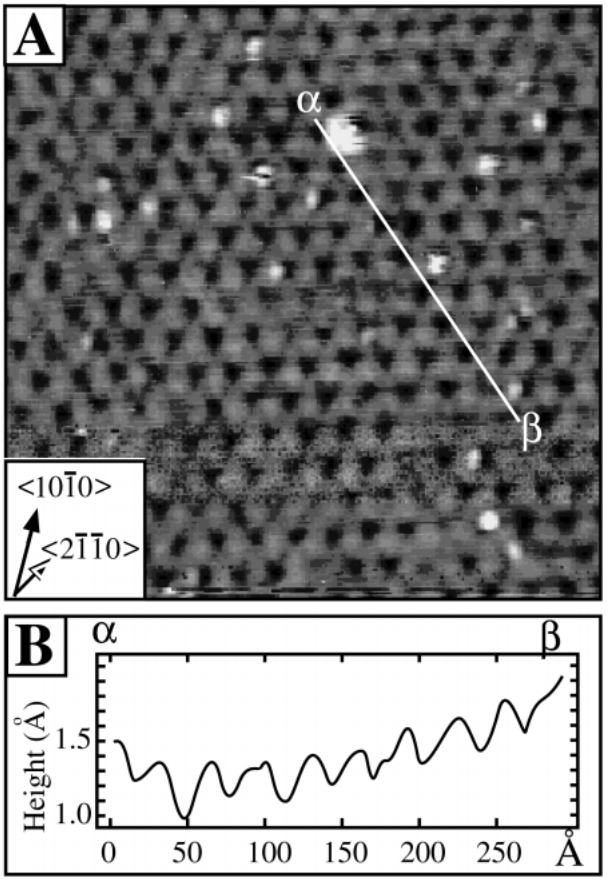


**FIGURE 6.** (**A**) A 500 × 500 Å constant current (sample bias 2.5 V, tunneling current 0.60 nA) STM image of an $FeTiO_3$ (0001) surface showing a moiré pattern. The image was obtained by annealing the sample at 1373 K in vacuum for 5 minutes, followed by 15 minutes $Ar^+$ sputtering and final annealing at 1373 K for 30 minutes in $1 \times 10^{-6}$ mbar $O_2$. The moiré pattern shows hexagonal symmetry, the periodicity of the structure being 29.2 ± 2.5 Å. (**B**) Cross section of (**A**) along the line α-β showing the periodicity and a corrugation amplitude of 0.5 Å.

that occurring at the surfaces of partially reduced α-$Fe_2O_3$ (Condon et al. 1995) or $Fe_3O_4$ (Condon et al. 1997), where larger scale superstructures are also observed.

Examination of the $FeTiO_3$ (0001) STM images shows that the relative areas of the two different terrace types (X and Y in Fig. 4a) vary depending upon which part of the crystal is imaged. These differences in relative area may be due to variations in temperature or redox conditions at the crystal surface during the annealing process, or to the rate of cooling after the annealing cycle. Compared with α-$Fe_2O_3$, $FeTiO_3$ is stable at lower oxygen partial pressures. A α-$Fe_2O_3$ (0001) surface would rapidly reduce to $Fe_3O_4$ (111) (Condon et al. 1994) if prepared in a similar manner to that of the $FeTiO_3$ (0001) surface in these experiments. This rules out the possibility that the surfaces imaged were α-$Fe_2O_3$ (0001) surfaces.

**Higher resolution images**

An STM image (Fig. 7a) of the terrace labeled Y in Figure 4a, obtained after two cycles of a 15 minute $Ar^+$ sputter and annealing at 1473 K for 5 minutes, followed by a single annealing at 1373 K for 30 minutes in $1 \times 10^{-6}$ mbar $O_2$, shows features arranged in a hexagonal array, with a separation of 4.8 ± 0.2 Å. These dimensions are consistent with a (0001) termination of the $FeTiO_3$ bulk crystal as identified by the observed (1 × 1) LEED pattern (Fig. 2). A (0001) termination of the $FeTiO_3$ bulk crystal structure gives a surface unit-cell length of 5.089 Å.

A line section of this image (Fig. 7a) shows considerable variation in the heights of individual surface features. The corrugation height range is from ~0.2 to ~0.6 Å. A high density (~10%) of point defects at the crystal surface can also be ob-

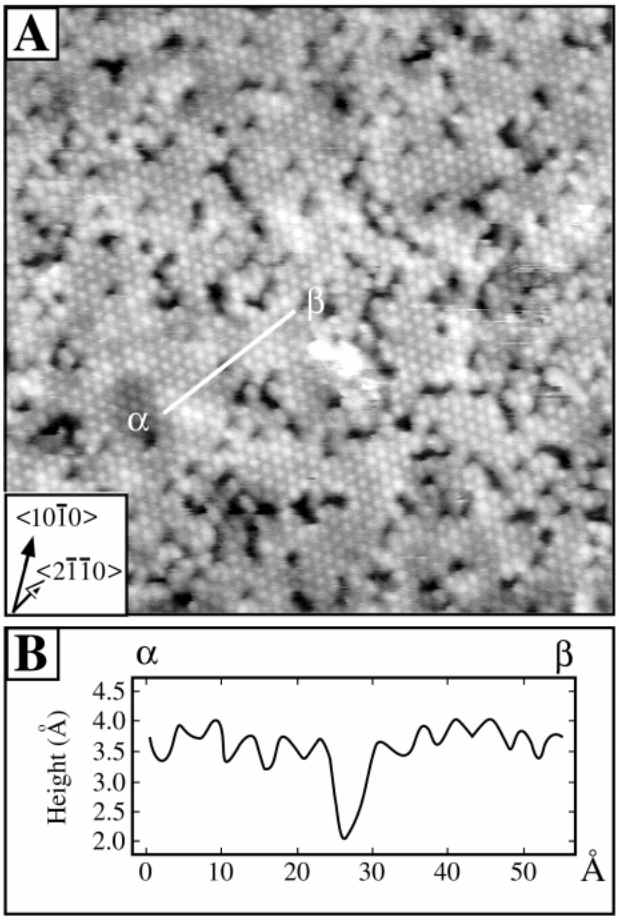


**FIGURE 7.** (**A**) A 200 × 200 Å constant current (sample bias –1.62 V, tunneling current 0.75 nA) STM image of an $FeTiO_3$ (0001) surface showing close-packed features. The image was obtained following two cycles of a 15 minute $Ar^+$ sputter and annealing at 1473 K for 5 minutes. The two cycles were then followed by a single annealing at 1373 K for 30 minutes in $1 \times 10^{-6}$ mbar $O_2$. During the annealing cycles, variations in temperature across the sample surface were observed as indicated by differences in radiance at different points on the sample surface. The bright features in the image are separated by a distance of 4.8 ± 0.2 Å, and a high density (~10%) of point defects can also be observed in the image. Multiple defects are preferentially aligned along [10$\bar{1}$0] and [01$\bar{1}$0] substrate directions. (**B**) Cross section of (**A**) along the line α-β showing the corrugation amplitude to be in the range of 0.2–0.6 Å. The section also shows the periodicity of the surface.

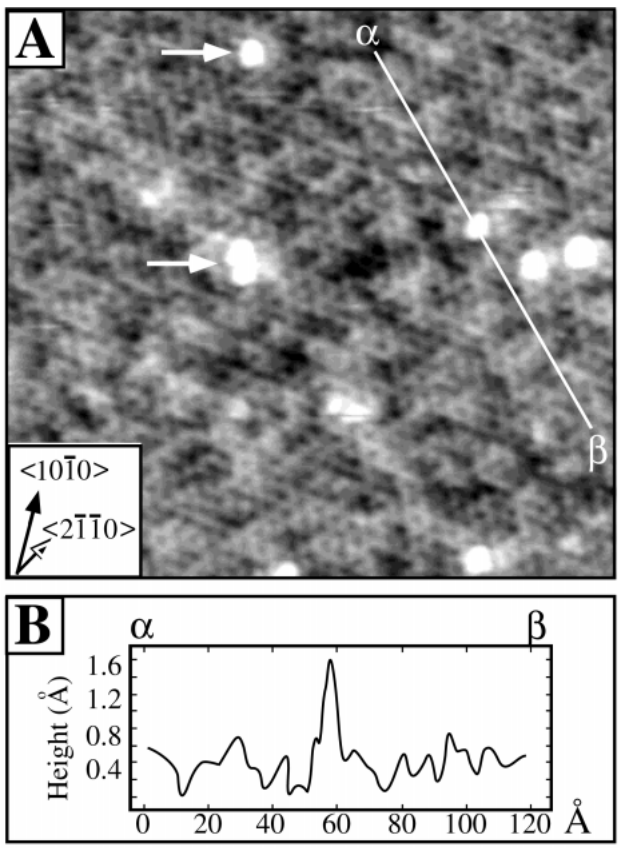


**FIGURE 8.** (**A**) A 200 × 200 Å constant current (sample bias –2.46 V, tunneling current 0.38 nA) STM image of an $FeTiO_3$ (0001) surface showing interconnecting ring-like features producing a honeycomb pattern. The image was obtained following annealing at 1473 K in vacuum for 10 minutes followed by a 15 minutes $Ar^+$ sputtering and final annealing at 1373 K for 30 minutes in $1 \times 10^{-6}$ mbar $O_2$. Distances between the centers of the rings are 4.7 ± 0.3 Å. Small amounts of surface contamination are indicated by white arrows. (**B**) Cross section of (**A**) along the line α-β showing the corrugation amplitude to be in the range of 0.2–0.6 Å.

served; these are commonly seen on oxide surfaces when high annealing temperatures have been used (Henrich and Cox 1994). Single and multiple defect features seem to be common, with some preferential alignment in the [10$\bar{1}$0] and [01$\bar{1}$0] crystallographic directions.

A second type of STM image taken from the same surface (Fig. 8a) appears to show new features, but still retains the hexagonal symmetry of the image in Figure 7a, with distances between "dark" centers of 4.7 ± 0.3 Å. We suggest that these features arise from either a change in the STM tip structure during imaging, or probing of different electronic states of the surface imaged in Figure 7a. Randomly arranged bright regions observed in this image lie ~1.0 Å above the average height of the other surface features (Fig. 8a) and are interpreted as surface contamination.

Similar STM images to those of Figure 7a and Figure 8a were obtained from the $FeTiO_3$ (0001) surface showing the second LEED pattern (Fig. 3). This LEED pattern is consistent with either a spinel-type (111) termination or a $(2/\sqrt{3} \times 2/\sqrt{3})$ R30° reconstruction (Fellows et al. 1997). A surface with areas of both a spinel-type (111) (or reconstructed-type) termination and the (1 × 1) $FeTiO_3$ bulk termination structure may have been produced by variations in temperature across the sample surface during the annealing process.

It is possible that the rough terraces labeled X, which we were unable to image at atomic resolution, may have a surface structure different from the (1 × 1) $FeTiO_3$ bulk termination, therefore contributing to the second LEED pattern. In the $FeTiO_3$ structure, $Ti^{4+}$ and $Fe^{2+}$ cations will have different af-

finities for oxygen at the surface resulting in different stabilities (or surface energies) of X and Y terraces. Thus the differing appearance of X and Y terraces in the STM images may be the result of preferential contamination by oxygen during annealing. We cannot therefore propose a definitive model for the reconstructed surface structure indicated by the second LEED pattern (Fig. 3) as we were unable to obtain atomic resolution imaging from the X terraces.

### Crystallographic relationships between the bulk structure of $FeTiO_3$ and the LEED and STM data

Using evidence from the location of imaged features, surface symmetry, and step height measurements, the STM images can be interpreted in terms of the bulk $FeTiO_3$ structure. The first LEED pattern observed for this surface (Fig. 2) has been interpreted as arising from a $(1 \times 1)$ unreconstructed $FeTiO_3$ (0001) surface unit cell. Bulk $FeTiO_3$ (0001) terminations show a $(1 \times 1)$ surface lattice that produces $p3$ symmetry (threefold rotation). Thus, we would expect features observed in the STM images to be related to the bulk structure of $FeTiO_3$.

The step height between terraces of the same type in high-resolution images is $4.4 \pm 0.5$ Å, with no single step heights of $2.2 \pm 0.3$ Å. This is probably due to extended annealing of the surface during preparation in which Y terraces have grown to cover the whole $FeTiO_3$ (0001) surface, therefore removing single steps at the surface. In the bulk $FeTiO_3$ structure, this distance ($4.4 \pm 0.5$ Å) corresponds to the distance between either two planes of low position $Fe^{2+}$ cations, or two planes of low position $Ti^{4+}$ cations perpendicular to the [0001] direction, and implies that only one type of cation termination is present. Thus, we expect to find a relationship between $Fe^{2+}$ or $Ti^{4+}$ (0001) cation layers in the bulk $FeTiO_3$ structure and the features observed in the STM images.

This behavior is similar to a model put forward for $Fe_3O_4$ (111) surfaces imaged using STM. $Fe_3O_4$ (111) images show two different terminations after initial preparation (annealing at 1173 K in $2 \times 10^{-7}$ mbar of $O_2$ for 30 minutes), with one termination proposed as Fe terminated, the other proposed as terminating in O atoms capping a Fe trimer. After annealing at a higher temperature (1200 K in $1 \times 10^{-7}$ mbar of $O_2$ for 30 minutes), however, only large terraces of the Fe termination are imaged giving a double step from terrace to terrace (Lennie et al. 1996).

In the bulk $FeTiO_3$ structure, close-packed O layers in the (0001) plane have O-O distances of 2.3 Å. The features observed in the STM images shown in Figures 7a and 9a are separated by a distance of $4.8 \pm 0.2$ Å. Furthermore, the features in the image are rotated 30° from the O-array unit-cell vectors, as determined by Laue diffraction and LEED. Thus, feature-feature distances and surface unit-cell orientation eliminate the close-packed O layer arrangement as single contributors to the features in these STM images. Positioning within each bulk $Fe^{2+}$ or $Ti^{4+}$ (0001) cation plane of the $FeTiO_3$ structure can be high or low (Fig. 1). Therefore, if we take into account all of the cations (high and low) in a (0001) plane, the distance between cations would be identical to the O-O distance given above. This tends to rule out a complete bulk cation layer as the contributing source (electronic and atomic) of the features in this STM image. If, however, the (0001) surface of $FeTiO_3$ is terminated between the high and low position cations in a (0001) cation plane, the resulting cation (Fe or Ti) surface termination would have half the bulk layer cations in the low position only (Fellows et al. 1997). In $\alpha$-$Fe_2O_3$, which has a similar electronic and atomic structure to ilmenite, calculations show that

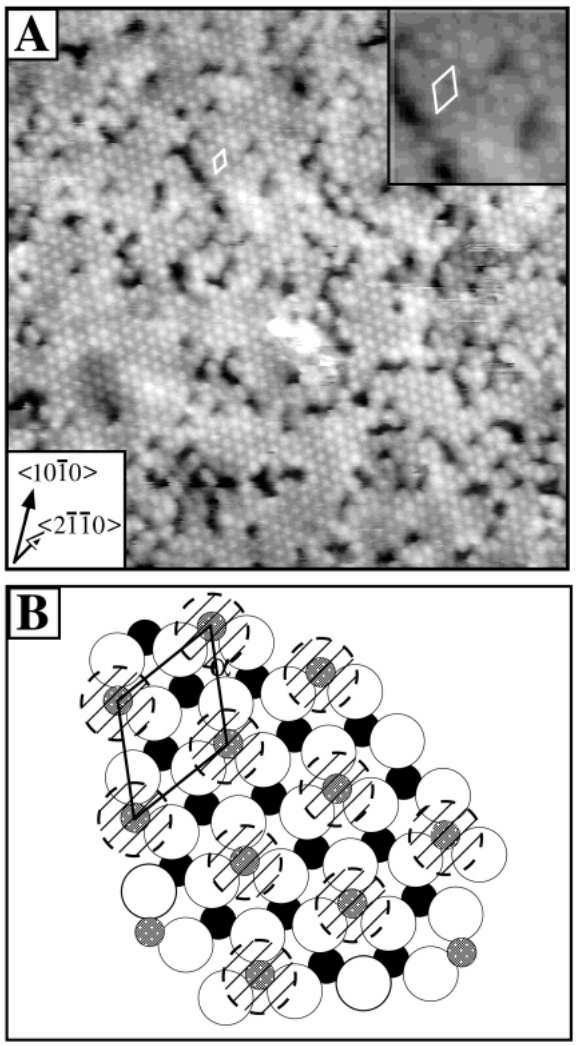


**FIGURE 9.** (**A**) A $200 \times 200$ Å constant current (sample bias –1.62 V, tunneling current 0.75 nA) STM image of an $FeTiO_3$ (0001) surface showing close-packed features. The image was obtained following the preparation described in Figure 7. The bright features in the image are separated by a distance of $4.8 \pm 0.2$ Å, and a high density (~10%) of point defects can also be observed in the image. Multiple defects are preferentially aligned along [10$\bar{1}$0] and [01$\bar{1}$0] substrate directions. An expanded part of the image ($30 \times 30$ Å) is shown in the top right-hand corner. (**B**) Schematic illustration of the low cation (0001) termination of $FeTiO_3$ obtained by lattice projection of the bulk structure. High-positioned cations in the bulk surface cation layer have been omitted. The black circles represent Fe or Ti atoms, gray circles represent Ti or Fe atoms and the large open circles are O anions. The oxygen trimers with capping cation (Fe or Ti) are shown with a dashed circle indicating the observed features in the first type of STM image. The hexagonal unit cell has edge dimensions of 5.089 Å.

this (0001) termination is the only thermodynamically stable surface (Becker et al. 1996). It has the lowest surface dipole moment, and is stabilized by relaxation of surface cations into the triangle of surrounding oxygen atoms. This cation termination in $FeTiO_3$ (0001) would give a cation-cation distance of 5.089 Å, which is consistent with the feature-feature distances of 4.8 ± 0.2 Å measured in the STM image. The orientation of features is also consistent with the bulk cation (Fe or Ti) lattice unit-cell vectors, as determined from Laue diffraction and LEED data. A model showing the low cation (0001) termination plane is given in Figure 9a, with features observed in STM images shown by dashed circles.

The second type of STM image (Figs. 8a and 10a) shows bright rings with dark centers separated by 4.7 ± 0.3 Å. This distance equals that between bright features in STM images shown in Figures 7a and 9a. The location of dark centers coincides with that of bright features in the first type of STM image, indicating a relationship between the two image types. This effect may be due either to a change in the tip structure during scanning, or probing a different part of the surface electronic structure following a change in the bias voltage (–1.62 V for bright centers, –2.46 V for dark centers). The bulk $FeTiO_3$ (0001) structure has a honeycomb arrangement of cations (Fe or Ti) lying below the "low" cation (0001) surface termination. We suggest that STM images with dark centers may arise from this underlying structure, and show a model for this structure in Figure 10a. This model also shows that in the center of each ring there is a "low" surface cation from the half-filled cation layer thought to produce the bright features seen in the first type of STM image.

Considering these models for the two STM image types, we note that features that would correspond to a close packed O-layer lying between the "low" cation surface layer and the bulk cation layer underneath do not appear in either of the STM image types (Figs. 7a and 9a). The STM images presented here can be compared to negative bias (–0.3 V) STM images of the $\alpha$–$Fe_2O_3$ (0001) surface taken in air (Eggleston and Hochella 1992), which show a close-packed array of features with a separation of 2.95 Å arranged parallel to the substrate O-array. These features have been modeled (Becker et al. 1996) as regions of high electronic valence-band density located above Fe atoms, with varying contributions of states with Fe 3d and O 2p character. Thus, a surface layer of "low" Fe cations, combined with the underlying Fe cations in the second layer, provide the arrangement that gives a close-packed array of features in the $\alpha$–$Fe_2O_3$ (0001) images of Eggleston and Hochella (1992).

In contrast, the $FeTiO_3$ (0001) STM images here appear to show the "low cation" arrangement at the surface (Fig. 9a) and, separately, depending on the bias voltage, the underlying cation arrangement (Fig. 10a). Differences in intensity and feature arrangement between images $\alpha$–$Fe_2O_3$ (0001) and $FeTiO_3$ (0001) would be expected due to the change in metal cation type in the layer below the oxygen.

These are the first high-resolution scanning tunneling microscopy images of the surfaces of a mixed iron-titanium oxide mineral. They show that the diversity of surface structures previously demonstrated for binary iron oxide minerals extends to the ternary oxides and, in particular, that more than one type of (0001) surface termination is possible for ilmenite ($FeTiO_3$). These experimental results provide an important reference for attempts to model the reactivity and electronic structure of ilmenite ($FeTiO_3$) surfaces.

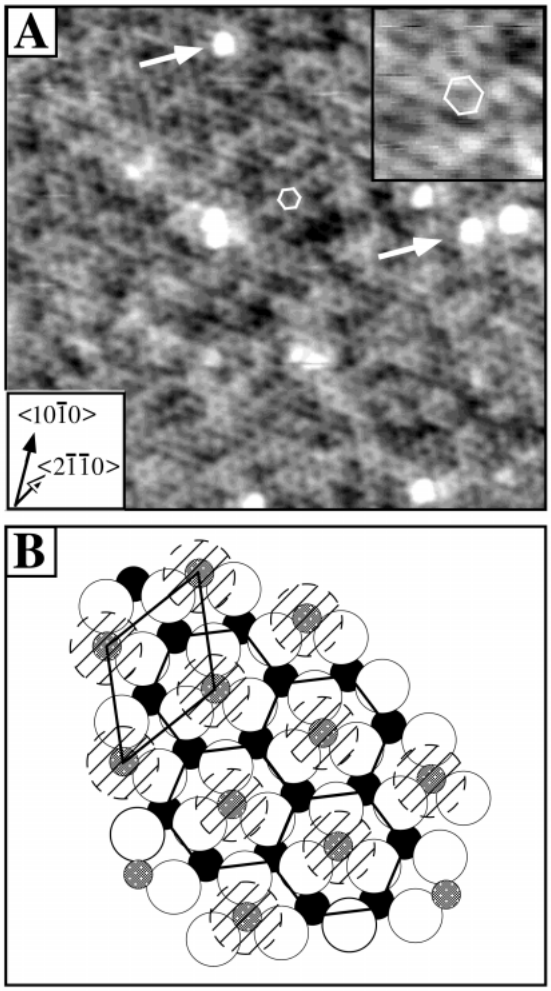


**FIGURE 10.** (**A**) A 200 × 200 A constant current (sample bias –2.46 V, tunneling current 0.38 nA) STM image of an $FeTiO_3$ (0001) surface showing interconnecting rings. The image was obtained following the preparation given in Figure 8. Distances between the centers of the rings are 4.7 ± 0.3 Å. Small amounts of surface contamination are indicated by white arrows. An expanded part of the image (30 × 30 Å) is shown in the top right-hand corner. (**B**) Schematic illustration of the low cation (0001) termination of $FeTiO_3$ obtained by lattice projection of the bulk structure. See Figure 9 for symbols. The lower bulk cation (Fe or Ti) layer produces a network of interconnecting hexagons. Features characteristic of the first type of STM image are shown as dashed circles and are positioned directly at the center of each hexagonal ring.

## ACKNOWLEDGMENTS

The authors thank the Swedish Museum of Natural History, Stockholm, for providing the $FeTiO_3$ single crystal used in this study (Museum reference no. 40:0050). This work was funded by NERC (grant no. GR/08549) including the award of a studentship to R.A.F. (GT4/95/225/E) and a postdoctoral fellowship to A.R.L., and by EPSRC (U.K.).

## REFERENCES CITED


Andreozzi, G.B., Cellucci, F., and Gozzi, D. (1996) High-temperature electrical conductivity of $FeTiO_3$ and ilmenite. Journal of Materials Chemistry, 6, 987–991.

Becker, U., Hochella, M.F., and Apra, E. (1996) The electronic structure of hematite {001} surfaces: Applications to the interpretation of STM images and heterogeneous surface reactions. American Mineralogist, 81, 1301–1314.

Berkó, A. and Solymosi, F. (1996) Study of $TiO_2$ (110) surface by scanning tunneling microscopy and spectroscopy. Langmuir, 12, 1275–1261.

Brown, N.E. and Navrotsky, A. (1993) Hematite-ilmenite ($Fe_2O_3$-$FeTiO_3$) solid solutions: Determinations of Fe-Ti order from magnetic properties. American Mineralogist, 78, 941–951.

Chevrier, J., Huang, L., Zeppenfeld, P., and Comsa, G. (1996) Characterisation by scanning tunneling microscopy of the oxygen induced restructuring of Au (111). Surface Science, 355, 1–12.

Condon, N.G., Murray, P.W., Leibsle, F.M., Thornton, G., Lennie, A.R., and Vaughan, D.J. (1994) $Fe_3O_4$ (111) termination of $\alpha$-$Fe_2O_3$ (0001). Surface Science, 310, L609–L613.

Condon, N.G., Leibsle, F.M., Lennie, A.R., Murray, P.W., Vaughan, D.J., and Thornton, G. (1995) Biphase ordering of iron-oxide surfaces. Physical Review Letters, 75, 1961–1964.

Condon, N.G., Leibsle, F.M., Parker, T., Lennie, A.R., Vaughan, D.J., and Thornton, G. (1997) Biphase ordering on $Fe_3O_4$ (111). Physical Review B—Condensed Matter, 55, 15885–15894.

Coulman, D.J., Wintterlin, J., Behm, R.J., and Ertl, G. (1990) Novel mechanism for the formation of chemisorption phases: The $(2 \times 1)$ O – Cu (110) "Added-Row" reconstruction. Physical Review Letters, 64, 1761–1764.

Eggleston, C.M. and Hochella, Jr., M.F. (1992) The structure of hematite (001) surfaces by scanning tunneling microscopy: Image interpretation, surface relaxation, and step structure. American Mineralogist, 77, 911–922.

Fellows, R.A., Lennie, A.R., Vaughan, D.J., and Thornton, G. (1997) A LEED study of the $FeTiO_3$ (0001) surface following annealing in $O_2$ partial pressures. Surface Science, 383, 50–56.

Gai, Z., He, Y., Li, X., Jia, J.F., and Yang, W.S. (1996) Application of Moiré fringes in investigations of subsurface imperfection—a study of dislocations and strain fields under the reconstructed surface layer of Au (001) by scanning tunneling microscopy. Surface Science, 365, 96–102.

Galloway, H.C., Sautet, P., and Salmeron, M. (1996) Structure and contrast in scanning tunneling microscopy of oxides: FeO monolayer on Pt (111). Physical Review B, 54, R11145–R11148.

Henrich, V.E. and Cox, P.A. (1994) The surface science of metal oxides, p69–72, Cambridge University Press, Cambridge.

Kim, Y.J., Westphal, C., Ynzunza, R.X., Galloway, H.C., Salmeron, M., Van Hove, M.A., and Fadley, C.S. (1997) Interlayer interactions in epitaxial oxide growth: FeO on Pt(111). Physical Review B, 55, R13448–R13451.

Klein, C. and Hurlbut, Jr., C. (1993) Manual of mineralogy (21st Edition), p380, Wiley, New York.

Kobayashi, K. (1996) Moiré patterns in scanning tunneling microscopy images of layered materials. Journal of Vacuum Science and Technology B, 14, 1075–1078.

Land, T.A., Michely, Th., Behm, R.J., Hemminger, J.C., and Cosma, G. (1992) STM investigation of single layer graphite structures produced on Pt (111) by hydrocarbon decomposition. Surface Science, 264, 261–270.

Leibsle, F.M., Murray, P.W., Condon, N.G., and Thornton, G. (1997) Scanning tunneling microscopy studies of reactions on metal surfaces and model oxide supports. Journal of Physics D—Applied Physics, 30, 741–756.

Lennie, A.R., Condon, N.G., Leibsle, F.M., Murray, P.W., Thornton, G., and Vaughan, D.J. (1996) Structures of $Fe_3O_4$ (111) surfaces observed by scanning tunneling microscopy. Physical Review B, 53, 10244–10253.

Lindsley, D.H. (1976a) The crystal chemistry and structure of oxide minerals as exemplified by the Fe-Ti oxides. In Mineralogical Society of America Reviews in Mineralogy, 3, L1–L52.

———(1976b) Experimental studies of oxide minerals. In Mineralogical Society of America Reviews in Mineralogy, 3, L61–L84.

Murray, P.W., Leibsle, F.M., Muryn, C.A., Fisher, H.J. Flipse, C.F.J., and Thornton, G. (1994) Interrelationship of structural elements on $TiO_2$ (100) – $(1 \times 3)$. Physical Review Letters, 72, 689–692.

Ritter, M., Over, H., and Weiss, W. (1997) Structure of epitaxial iron oxide films grown on Pt (100) determined by low energy electron diffraction. Surface Science, 371, 245–254.

Ritter, M., Ranke, W., and Weiss, W. (1998) Growth of ultrathin FeO films on Pt (111) studied by STM and LEED. Physical Review B, 57, 7240–7251.

Shirane, G., Pickart, J., Nathans, R., and Ishikawa, Y. (1959) Neutron-diffraction study of antiferromagnetic $FeTiO_3$ and its solid solution with $\alpha$-$Fe_2O_3$. Journal of Physics and Chemistry of Solids, 10, 35–43.

Waite, T.D. (1990) Photo-redox processes at the mineral-water interface. In Mineralogical Society of America Reviews in Mineralogy, 23, 559.

Weiss, W., Barbieri, A., Van Hove, M.A., and Somorjai, G.A. (1993) Surface structure determination of an oxide film grown on a foreign substrate: $Fe_3O_4$ multilayer on Pt (111) identified by low energy electron diffraction. Physical Review Letters, 71, 1848–1851.

Weiss, W. (1997) Structure and composition of thin epitaxial iron oxide films grown onto Pt (111). Surface Science, 377–379, 943–947.

Wiederholt, T., Brune, H., Wintterlin, J., Behm, R.J., and Ertl, G. (1995) Formation of two-dimensional sulfide phases on Al (111)—An STM study. Surface Science, 324, 91–105.


MANUSCRIPT RECEIVED APRIL 24, 1998
MANUSCRIPT ACCEPTED APRIL 13, 1999
PAPER HANDLED BY GLENN A. WAYCHUNAS